J Mater Sci (2007) 42:9163–9169
DOI 10.1007/s10853-007-1926-x

Electrochemical deposition of Ni and Cu onto monocrystalline *n*-Si(100) wafers and into nanopores in Si/SiO_2 template

Yu. A. Ivanova · D. K. Ivanou · A. K. Fedotov · E. A. Streltsov · S. E. Demyanov · A. V. Petrov · E. Yu. Kaniukov · D. Fink

Received: 16 January 2007 / Accepted: 7 June 2007 / Published online: 28 July 2007
© Springer Science+Business Media, LLC 2007

Abstract Nickel and copper were potentiostatically deposited onto monocrystalline *n*-Si (100) wafers and in nanoporous SiO_2/Si template from 0.5 M $NiSO_4$ + 0.5 M H_3BO_3 and 0.005 M $CuSO_4$ + 0.5 M H_3BO_3 solutions. Nanoporous SiO_2/Si template was formed by etching in dilute HF solution of ion tracks. The latter were produced by high-energy (380 MeV) Au^+ ions bombardment of silicon oxide thermally grown on silicon (100) substrate. The deposition of metals was studied using cyclic voltammetry (CV), chronoamperometry; the structure and morphology of products were ex-situ investigated by SEM and XRD. The level of pores filling was controlled by deposition time. Electrodeposition occurred selectively into nanopores and the deposition on SiO_2 layer was excluded. It was found out that Ni and Cu electrodeposited into nanopores of SiO_2/Si system formed the same structures as at electrodeposition on the surface of monocrystalline *n*-Si—granules for Ni and scale-shaped particles for Cu deposits.

Y. A. Ivanova · D. K. Ivanou · A. K. Fedotov · E. A. Streltsov (✉)
Chemistry Department, Belarusian State University, Leningradskaya st. 14, 220050 Minsk, Belarus
e-mail: streltea@bsu.by

S. E. Demyanov · A. V. Petrov · E. Y. Kaniukov
Joint Institute of Solid State and Semiconductor Physics, NASB, 19 P.Brovka Str, 220072 Minsk, Belarus

D. Fink
Hahn-Meitner-Institute, 100 Glienicker Str, 14109 Berlin, Germany

Introduction

In recent years, the stable growth of costs for developing of new technologies for producing of electronic devices composed of very small active elements (down to several nanometers) is observed. Monocrystalline silicon is known to be the main material for modern electronics. In this connection the investigations of processes for deposition of various nanostructures (magnetic, nonmagnetic and semiconductor as well) onto Si surface for electronic nanodevices (transistors, emitters, sensors, photoresistors, etc.) production are of great interest.

As a result the technique of tracks formation under swift heavy ions implantation for electronic nanodevices manufacturing is under consideration nowadays [1, 2]. First of all, it is interesting to use etched tracks in SiO_2 grown on monocrystalline Si wafer [3]. The chemical etching of the latent tracks in SiO_2 layer on Si substrate (SiO_2/Si) results in formation of through nanopores suitable for filling with different substances such as metals, polymers, semiconductors, etc. being in direct contact with Si [3–6]. Filled nanopores in SiO_2 layer on Si wafer are of particular interest as the intermediate structures between traditional silicon-based microelectronic devices and nanoelectronic ones [4, 6].

The chemical deposition is the most widely used method for metal deposition into nanopores in SiO_2. Usually the solution containing both the metal coordination compound and reducing agent is used. The rate of deposition is controlled by the concentration of the reagents and the ligand nature. The latter also effects on the difference of redox potentials. However, the method does not possess the selectivity—the deposition occurs both into pores and onto the SiO_2 surface [5, 6]. We have previously shown that this problem could be solved by using the electrochemical

deposition technique. Particularly, CdTe and PbSe were electrochemically deposited into pores of SiO_2/Si system [7, 8]. We have proved that the deposition takes place only into pores and could be easily controlled by the electrode potential.

In the present work electrochemical deposition of Ni and Cu on *n*-Si wafers and into nanopores in SiO_2 layer formed on *n*-Si(100) wafers has been studied.

Experimental

Cu and Ni were electrochemically deposited into porous SiO_2 layer grown on *n*-Si (100) wafers (P-doped with resistivity of 4.5 Ω cm). For comparison Cu und Ni electrodeposition onto the surface of monocrystalline *n*-Si (100) wafers was also studied. Prior to the electrochemical experiments the samples of Si substrates were subsequently cleaned in HNO_3 (weight percentage $w = 56\%$) at 80 °C during 30 s, washed by bidistilled water and etched in HF ($w = 4\%$) to remove the native surface oxide and to form atomically smooth hydrogen-activated (H-terminated) surface [9, 10]. To produce porous SiO_2/Si template, SiO_2 layer was thermally grown on *n*-Si (100) substrate at 1,100 °C during 10 h in oxygen atmosphere. The initial thickness of grown SiO_2 layer was found to be 0.9 ± 0.1 μm. Then the samples were irradiated by scanned beams of 350 MeV $^{197}Au^{+}$ ions with fluence of 5×10^{8} cm^{-2} at the "ISL" accelerator center at the Hahn-Meitner-Institute (Berlin, Germany) to produce latent ion tracks in silicon oxide. Pores were formed under chemical etching of the irradiated SiO_2 layer in dilute HF ($w = 1.35\%$). Electrical contact to Si substrates was performed through In–Ga eutectic.

Electrochemical and photoelectrochemical measurements were carried out in a three-electrode two-compartment cell (the cell volume was 20 cm^3) with an optical quality window, platinum counter-electrode and Ag, $AgCl|KCl_{(sat.)}$ reference electrode (+0.220 V versus saturated hydrogen electrode). All potentials in the work are given with respect to this reference electrode. The potentials were controlled by the conventional programmable potentiostate. The potential scan rate was 0.02 V s^{-1} in all potentiodynamic experiments.

Metal electrodeposition was carried out in solution 0.5 M $NiSO_4$ + 0.5 M H_3BO_3 (Ni bath); 0.005 M $CuSO_4$ + 0.5 M H_3BO_3 (Cu bath). The electrolytes were prepared using high purity reagents and bidistilled water.

Before electrochemical measurements the electrolytes were deaerated by Ar during 10 min. During all experiments Ar flow was kept above the electrolyte in the cell. The halogen lamp (50 W, 12 V) with IR filter was used as a light source. The light flux power $J = 7$ mW cm^{-2}. The experiments were carried out at constant temperature of 20 ± 2 °C.

Scanning electron microscopy (SEM) investigations were performed with LEO 1455 microscope (ROENTEC GmbH). X-ray diffraction (XRD) analysis was carried out with HZG-4A diffractometer using CoKα radiation and MnO_2 filter.

Results and discussion

Nanopores formation in SiO_2/Si template

The nanoporous SiO_2/Si template was formed under chemical etching of the irradiated SiO_2 layer in dilute HF at ambient conditions. During the etching the dissolution of SiO_2 layer occurs. The damaged regions (latent tracks) contain a lot of defects like distorted and broken bonds, point defects, etc. and their chemical activity is higher when compared with nondamaged ones. Therefore, the etching rate of latent tracks in SiO_2 is higher than non-damaged areas and cone-shaped pores are formed. The etching was characterized in terms of changing of SiO_2 layer thickness d and pores' parameters (the diameter d_{top}

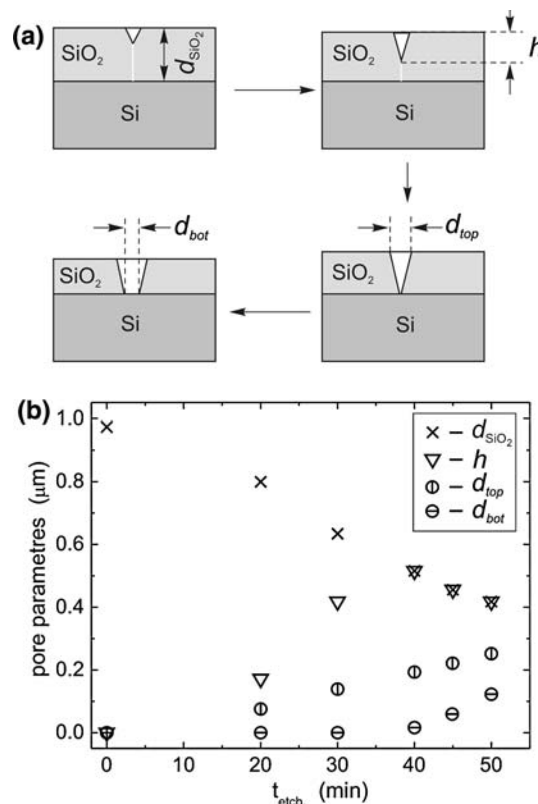

Fig. 1 The scheme showing the stages of etching of latent tracks in SiO_2 layer on *n*-Si surface in HF solution (**a**) and the pore parameters versus the etching time in 1.35% HF solution at 20 °C (**b**)

of pore top part, the bottom pore diameter d_{bot} and the pore height h) (Fig. 1a). While etching the top pore diameter rises and through pore with bottom diameter d_{bot} is formed at etching time $t_{etch} > 30$ min (Fig. 1b). As experiments have shown, the pore height h rised at first stage of etching and then decreased with time due to thinning of SiO_2 layer.

In order to obtain SiO_2/Si template with pores suitable for electrochemical filling it is necessary to carry out the etching process till the uncapping of Si surface, since electrodeposition is realized only onto conducting areas of a template. It was observed that etching for 45 min caused the formation of pores randomly distributed over the surface and looked like truncated cones with the base diameters of 110 and 250 nm and height h of about 430 nm (see Fig. 2).

Before filling of pores in SiO_2/Si templates by metals, the characteristic features of metal deposition onto n-Si surface in the mentioned electrolytes were preliminary investigated. Firstly, the electrochemical behavior of n-Si electrode in 0.5 M H_3BO_3 (background electrolyte) was studied.

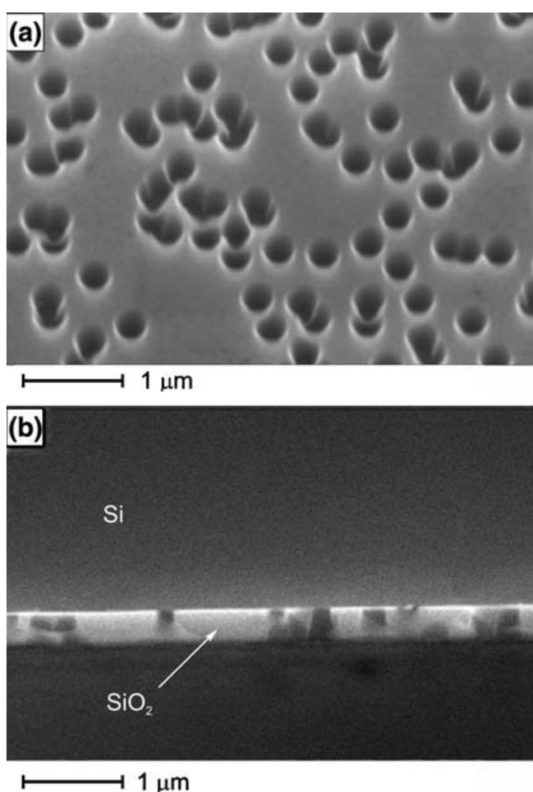

Fig. 2 SEM images of nanopores in SiO_2 layer after treating in 1.35% HF solution at 20 °C during 45 min: top view (**a**) and cross section under 30° (**b**)

Electrochemical behavior of n-Si electrode in H_3BO_3

Figure 3 presents the voltammogram for n-Si electrode in 0.5 M H_3BO_3 (pH 3.7). Significant cathodic current appears at potentials $E \leq -0.8$ V. This current is associated with H^+ reduction. Under dark anodic polarization there is no remarkable anodic current on the CV curve down to +1.2 V. Provided n-Si electrode is illuminated, anodic photocurrent appears at $E \geq -0.25$ V. This current is related to the silicon oxidation and results in formation of insulating $SiO_2 \cdot nH_2O$ layer on the electrode surface. The following cathodic potential scan does not exhibit any cathodic current within the range of potentials from 0 to –1.2 V. Such an electrochemical behavior of n-Si in H_3BO_3 solution is in a good agreement with a band bending model. Cathodic processes on n-Si occur at potentials E less than flat band potential of the semiconductor (E_{fb}). At potentials $E > E_{fb}$ space charge region (SCR) is formed in n-Si preventing its oxidation in the dark. Under illumination photoelectrons and photoholes are generated in silicon. SCR separates photoelectrons and photoholes. Photoholes move towards n-Si surface and take part in the oxidation resulting in anodic photocurrent. As a first approximation the onset potential of anodic photocurrent $E^a_{on} = -0.25$ V could be admitted to E_{fb} of semiconductor [11].

Nickel electrodeposition onto n-Si electrode and into porous SiO_2/Si template

In the H_3BO_3 electrolyte containing 0.5 M $NiSO_4$ the onset potential of the cathodic current is –0.80 V (Fig. 4a). This current is significantly higher than cathodic current on n-Si in background electrolyte and related to Ni(II) reduction on

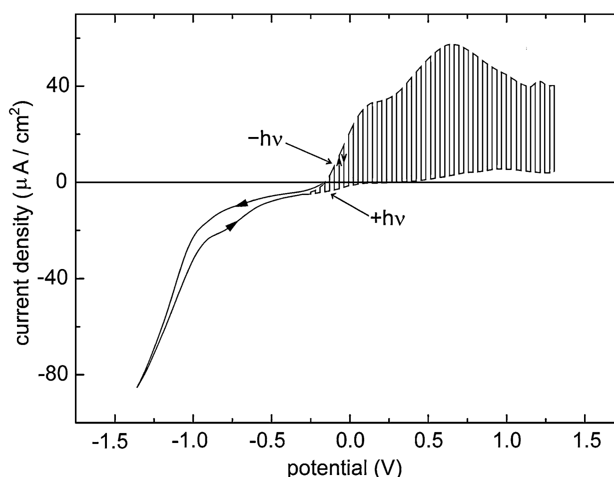

Fig. 3 Cyclic voltammograms for n-Si electrode in 0.5 M H_3BO_3 recorded under chopped illumination. The direction of potential scan is given by arrows

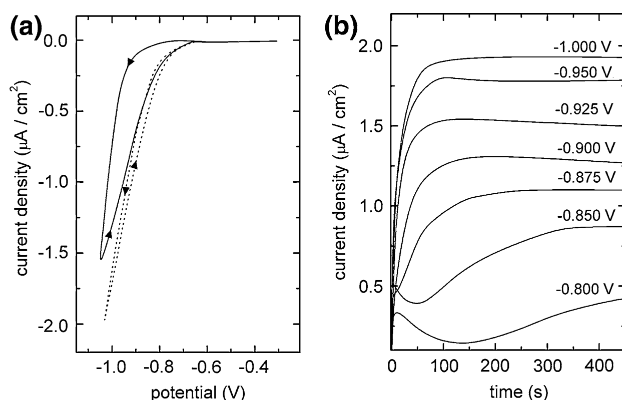

Fig. 4 Cyclic voltammogram (**a**) for *n*-Si electrode in 0.5 M H_3BO_3 + 0.5 M $NiSO_4$ (solid line—the first scan, dashed line—the second potential scan). Current–time transients (**b**) for nickel deposition onto *n*-Si in 0.5 M H_3BO_3 + 0.5 M $NiSO_4$. All the curves were recorded in the dark

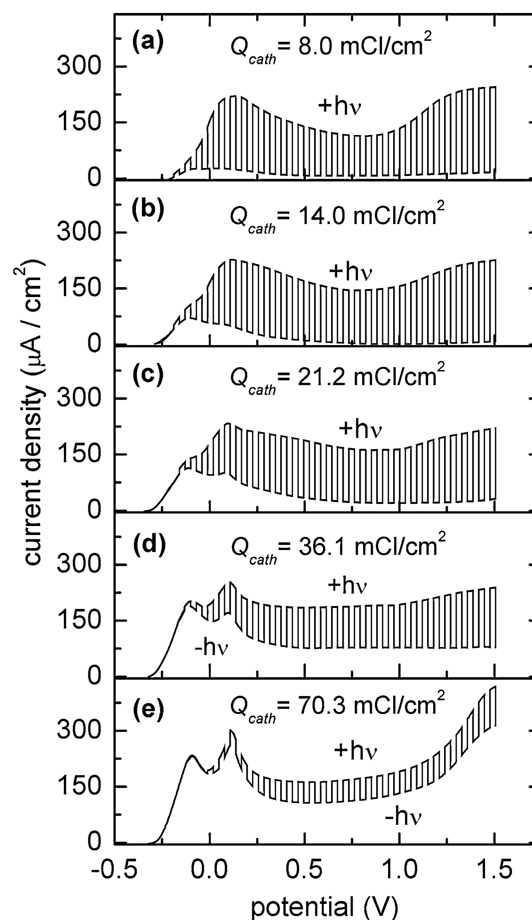

Fig. 5 Anodic voltammogram for *n*-Si/Ni electrode in 0.5 M H_3BO_3 + 0.5 M $NiSO_4$ recorded under chopped illumination. The values of cathodic charge responsible for Ni electrodeposition (at E = –1.0 V) are indicated on the plots

n-Si surface, which takes place with overvoltage η_c = 0.31 V. As the equilibrium potential of Ni(II) reduction E_{Ni^{2+}/Ni^0} = –0.49 V less than E_{fb}, the high overvoltage of Ni deposition onto *n*-Si is caused by the nucleation barrier. The reverse potential scan exhibits a narrow loop of current hysteresis, which points to 3D nuclei formation and autocatalytic character of Ni deposition as usual for metal deposition onto Si [12–15]. At the second cathodic potential scan nickel deposition takes place with lower overvoltage η_c' = 0.17 V. This fact indicates that Ni deposition occurs onto Ni nuclei formed on the silicon surface at the first cathodic potential scan. The reverse potential scan does not show any anodic current in the dark within the potential range from –1.0 to –0.32 V.

Figure 4b shows a series of current transients for Ni deposition onto *n*-Si electrode at constant potentials within the potential range from –0.80 to –1.00 V with step of 0.025 V. The stirring of the electrolyte does not exert upon the value of cathodic current but the level of cathodic polarization does: the more negative potential is applied the higher current appears. Therefore, at potential range from –0.80 to –1.00 V Ni deposition onto *n*-Si is kinetically limited.

Figure 5 presents the anodic voltammograms for *n*-Si electrode after Ni electrodeposition recorded under chopped illumination. As evident from the figure, the form of the curves differs depending on the amount of Ni electrodeposited. At small amounts of Ni (Fig. 5a) only the anodic photocurrent is observed for *n*-Si/Ni electrode. It is 3–5 times higher in comparison with bare *n*-Si and caused by Ni oxidation due to photoholes generated in *n*-Si under illumination.

As the quantity of Ni increases the dark anodic current appears. The greater the quantity of Ni deposit on the Si electrode, the greater dark current is registrated and the lower photocurrent is observed (Fig. 5b–e). According to these data we supposed that both dark anodic current and photocurrent on *n*-Si/Ni electrode are mainly attributed to Ni oxidation. The side reaction of *n*-Si oxidation also takes place under illumination. The immediate cause of such an electrochemical behavior of *n*-Si/Ni electrode is not fully clear. It is probably related to the peculiarities of particles size distribution at different amounts of nickel that effects on the Me–substrate interaction and results in difference in anodic oxidation of *n*-Si/Ni electrode.

The increasing of anodic current at potentials $E \geq +1.1$ V is probably related to H_2O oxidation on *n*-Si/Ni electrode.

SEM images of *n*-Si electrode covered with Ni granules at E = –1.0 V are presented in Fig. 6a and b. At the first stages of deposition the individual roundish particles with sizes of 30–70 nm are formed. At longer time the deposit represents compact granular uniform coating. According to the XRD data face centered cubic (fcc) Ni phase with lattice parameter a = 0.352 nm is formed (Fig. 6e).

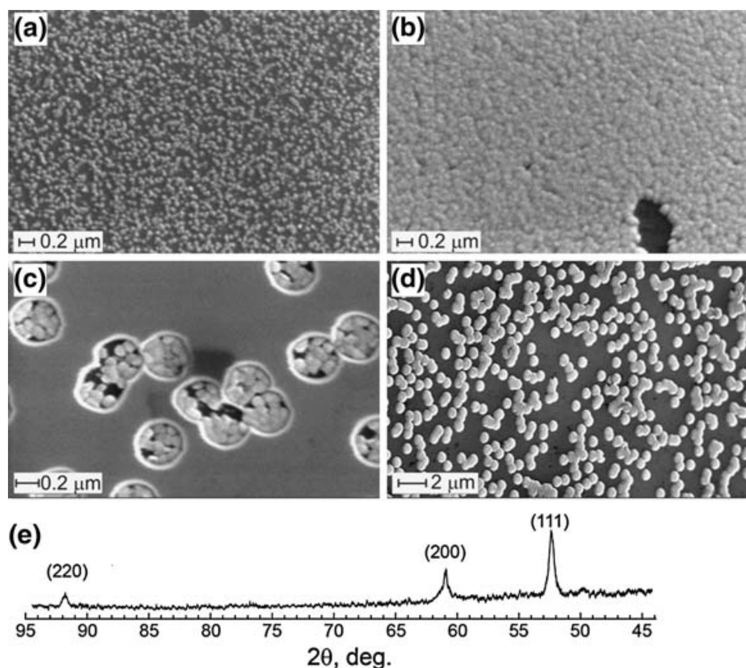

Fig. 6 SEM images of Ni particles electrodeposited onto *n*-Si surface for 30 s (**a**) and 120 s (**b**) and into nanoporous SiO_2/Si template for 40 s—at the pore bottom (**c**) and for 150 s—filled pores (**d**) and XRD pattern of Ni electrodeposited onto *n*-Si surface (**e**). Electrodeposition was carried out at $E = -1.0$ from electrolyte 0.5 M H_3BO_3 + 0.5 M $NiSO_4$

Being electrodeposited into nanopores in SiO_2/Si template, Ni also forms granules with sizes of 50–70 nm. First, Ni particles are formed at the pore bottom (Fig. 6c). In the course of deposition metal fills the pores entirely and forms caps at SiO_2/Si surface. In Fig. 6d one can see that there are no empty pores and all of them are simultaneously being filled with nickel.

Copper electrodeposition onto *n*-Si electrode and into porous SiO_2/Si template

In the H_3BO_3 electrolyte containing 0.005 M $CuSO_4$ cathodic current is showed up at potentials $E \leq -0.25$ V (Fig. 7) and caused by Cu nucleation and growth at *n*-Si surface. This process occurs with overvoltage $\eta_c = 0.30$ V. The overvoltage is related to SCR formation in *n*-Si at $E \geq E_{fb}$. Cathodic current peak is observed at $E = -0.65$ V indicating 3D nucleation followed by diffusion limited growth.

As in the case of nickel deposition, the voltammogram of Cu electrodeposition onto *n*-Si is characterized by cathodic current hysteresis loop being evidence of self-catalyzed process. On the reverse potential scan within the range of potentials from –1.5 to 1.2 V there is no anodic current in the dark. As it was already reported in [14, 16], the barrier for Cu oxidation at *n*-Si/Cu interface is formed.

Provided the electrode is being illuminated, anodic photocurrent on CV curve is registrated. This photocurrent is 4–5 times higher when compared with bare *n*-Si and is attributed to Cu oxidation.

A similar effect of anodic photocurrent increase was also observed for systems *n*-Si/Te and *n*-Si/PbTe. In these systems Te and PbTe are photoelectrochemically inactive components and do not exhibit anodic photocurrent. They act as effective acceptors of photoholes generated in *n*-Si substrate and contribute to photocurrent increase [17, 18].

Figure 8 presents a series of current transients obtained for Cu deposition onto *n*-Si within the potential range from –0.45 to –0.70 V. All the curves are characterized by initial current increase due to nucleation and subsequent current drop at longer time. These features indicate diffusion-limited process. In order to analyze the nucleation mechanism the deposition transient at $E = -0.50$ V was plotted in dimensionless form by normalizing two variables *j* and *t*

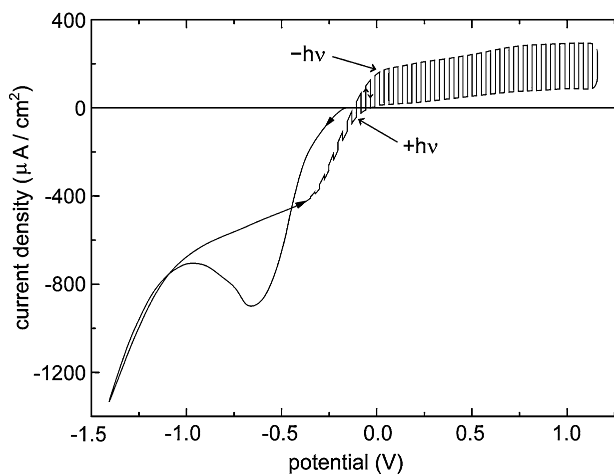

Fig. 7 Cyclic voltammogram for *n*-Si electrode in 0.5 M H_3BO_3 + 0.005 M $CuSO_4$ recorded under chopped illumination. The direction of potential scan is given by arrows

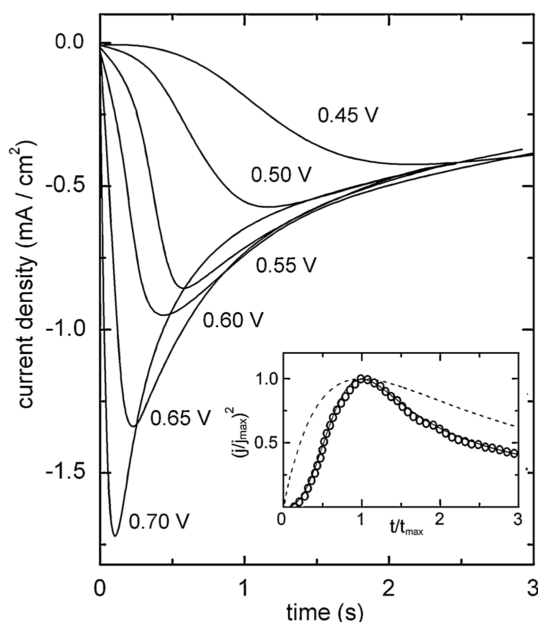

Fig. 8 Current–time transients for copper deposition onto *n*-Si in 0.5 M H_3BO_3 + 0.005 M $CuSO_4$ at different potentials recorded in the dark. The potentials applied are indicated on the plot. Inset—normalized current transient at E = –0.50 V plotted in dimensionless form (○); the theoretical curve for instantaneous (broken line) and progressive (solid line) nucleation

with respect to maximum current j_{max} and time t_{max} at which the maximum current was observed.

For instantaneous nucleation the theoretical normalized rate law is given by [19]:

$$\frac{j^2}{j_{max}^2} = 19,542\left(\frac{t_{max}-t_0}{t-t_0}\right)\left[1-\exp\left(-12,564\frac{t-t_0}{t_{max}-t_0}\right)\right]^2$$

For progressive nucleation the theoretical normalized rate law is given by [19]:

$$\frac{j^2}{j_{max}^2} = 12,254\left(\frac{t_{max}-t_0}{t-t_0}\right)\left[1-\exp\left(-23,367\frac{(t-t_0)^2}{(t_{max}-t_0)^2}\right)\right]^2$$

where t_0—induction time i.e. the time needed to form a nucleus lager than the critical nucleus size.

The theoretical plots for progressive and instantaneous nucleation and experimental plot for Cu(II) reduction at E = –0.50 V are given on inset in Fig. 8.

It could be seen that experimental deposition transient was in good agreement with the curve for progressive nucleation followed by diffusion-limited growth. These data are in close agreement with results obtained earlier for Cu deposition onto *n*-Si from sulphuric electrolytes [16, 20] and boric electrolyte with HF (HBF_4) additive [14, 21].

According to SEM images (Fig. 9a and b), Cu formed on *n*-Si represents plane scale-shaped particles with sizes of 30–300 nm. XRD data point to fcc Cu phase with a = 0.362 nm (Fig. 9e). Under the same conditions Cu electrodeposition into pores in SiO_2/Si template was realized. Plane particles were obtained at the bottom of pores at the first stages of deposition (Fig. 9c). With time Cu fills the pores entirely and structures composed of cross-cut particles are formed (Fig. 9d). As for Ni deposition into

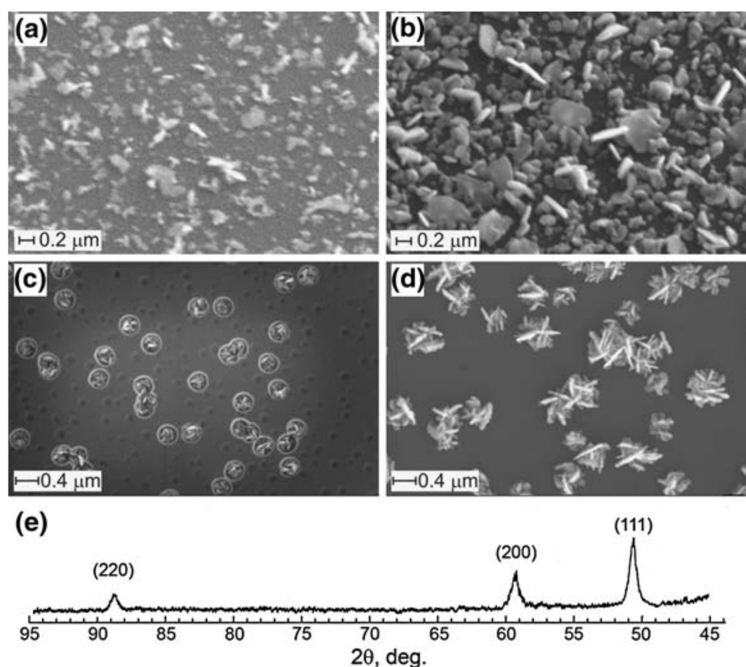

Fig. 9 SEM images of Cu particles electrodeposited onto *n*-Si during 30 s (**a**) and 120 s (**b**) and into nanoporous SiO_2/Si template during 40 s (**c**) and 150 s (**d**) and XRD pattern of Cu electrodeposited onto *n*-Si surface (**e**). Electrodeposition was carried out at E = –0.5 V from electrolyte 0.5 M H_3BO_3 + 0.005 M $CuSO_4$

SiO_2/Si template, Cu electrodeposition also occurs only into pores and template with all the pores uniformly filled with metal could be produced.

Conclusions

Nickel and copper were electrochemically deposited from boric solutions of metal sulphates onto the surface of monocrystalline *n*-Si(100) wafers and into nanopores in SiO_2/Si template. Metal deposition onto *n*-Si is characterized by 3D island growth mechanism. The data concerning the regimes of metal deposition onto *n*-Si surface were used to fill the pores in SiO_2/Si template by metallic nanoparticles. Being electrodeposited into nanopores of SiO_2/Si template, Ni and Cu represented nearly the same structures as they formed at the surface of monocrystalline *n*-Si—granules for Ni and scale-shaped particles for Cu. Electrodeposition permits selective formation of metals in nanopores—the deposition on insulating SiO_2 layer is prohibited. The level of pores filling was controlled by deposition time. The used electrodeposition technique allowed producing templates where all the pores were uniformly filled with metal.

Acknowledgement This work was supported by the Belarusian Foundation for Basic Research (Project X07M-128).

References

1. Fink D (2004) Fundamentals of ion-irradiated polymers. Springer Series in Materials Science, vol 63
2. Fink D, Alegaonkar PS, Petrov AV, Berdinsky AS, Rao V, Müller M, Dwivedi KK, Chadderton LT (2003) Radiat Measur 36:605
3. Fink D, Petrov AV, Hoppe K, Fahrner WR et al (2004) Nucl Instr Meth B218:355
4. Fink D, Alegaonkar PS, Petrov AV, Wilhelm M, Szimkowiak P, Behar M, Sinha D, Fahrner WR, Hoppe K, Chadderton LT (2005) Nucl Instr Meth B236:11
5. Sinha D, Petrov AV, Fink D, Fahrner WR, Hoppe K, Chandra A (2004) Radiat Effects Defects Solids 159:517
6. Fink D, Sinha D, Opitz-Coutureau J, Petrov AV, Demyanov SE, Fahrner WR, Hoppe K, Fedotov AK, Chadderton LT, Berdinsky AS (2005) In: Borisenko VE, Gaponenko SV, Gurin VS (eds) Physics, chemistry and application of nanostructures. World Scientific Pubs., p 474
7. Ivanou DK, Streltsov EA, Fedotov AK, Mazanik AV, Fink D, Petrov A, Tkazyk Z, Wosinski T, Figielski T (2005) In: Pődör B, Horváth J, Basa P (eds) Semiconductor nanocrystals (Proc. of the 1st Intern. Workshop on Semicond. Nanocrystals "SEMINANO-2005", Budapest, Hungary, September 2005), p 63
8. Ivanou DK, Streltsov EA, Fedotov AK, Mazanik AV, Fink D, Petrov A (2005) Thin Solid Films 490:154
9. Ubara H, Imura T, Hiraki A (1984) Solid State Commun 50:673
10. Niwa D, Takano N, Yamada T, Osaka T (2003) Electrochim Acta 48:195
11. Gurevich YuYa, Pleskov YuV (1983) Photoelektrokhimija poluprovodnikov. Nauka, Moscow, p 176 (in Russian)
12. Rashkova B, Guel B, Pötzschke RT, Staikov G (1998) Electrochim Acta 43:3021
13. Munoz AG (2006) Surf Coat Technol 201:3030
14. Oskam G, Long JG, Natarajan A, Searson PC (1998) J Phys D: Appl Phys 31:1927
15. Pasa AA, Munford ML, Voltolini E, Seligmana L, Sardelab M, Sartorelli ML (2001) In: Proceedings of the magnetic materials, processes, and devices VI. The Electrochemical Society, vol 2000, p 137
16. Ji C, Oskam G, Searson PC (2001) Surf Sci 492:115
17. Ivanova YuA, Ivanou DK, Streltsov EA (2007) Electrochem Commun 9:599
18. Ivanova YuA, Ivanou DK, Streltsov EA (2007) Electrochim Acta 52:5213
19. Gunawardena G, Hills G, Montenegro I, Scharifker B (1982) J Electroanal Chem 138:225
20. Krumm R, Guel B, Schmitz C, Staikov G (2000) Electrochim Acta 45:3255
21. Pasa AA, Scharzacher W (1999) Phys Stat Sol(a) 173:73